REPORT DOCUMENTATION PAGE

Form Approved
OMB No. 0704-0188

PLEASE DO NOT RETURN YOUR FORM TO THE ABOVE ORGANIZATION.

1. REPORT DATE *(DD-MM-YYYY)*	2. REPORT TYPE	3. DATES COVERED *(From - To)*
29/02/2012	Final Report	06/01/2009-11/30/2011

4. TITLE AND SUBTITLE
INTEGRATION OF MODEL-BASED ESTIMATION THEORY WITH AN ADAPTIVE FINITE VOLUME METHODS FOR THE DETECTION OF A MOVING GASEOUS SOURCE VIA A MOBILE SENSOR

5a. CONTRACT NUMBER

5b. GRANT NUMBER
FA9550-09-1-0469

5c. PROGRAM ELEMENT NUMBER

6. AUTHOR(S)
Michael A. Demetriou and Nikolaos A. Gatsonis

5d. PROJECT NUMBER

5e. TASK NUMBER

5f. WORK UNIT NUMBER

7. PERFORMING ORGANIZATION NAME(S) AND ADDRESS(ES)
Worcester Polytechnic Institute
100 Institute Rd.
Worcester, MA, 01609

8. PERFORMING ORGANIZATION REPORT NUMBER

9. SPONSORING/MONITORING AGENCY NAME(S) AND ADDRESS(ES)
AFOSR
875 N. Randolph Street
Suite 325, RM 3112

10. SPONSOR/MONITOR'S ACRONYM(S)

11. SPONSOR/MONITOR'S REPORT NUMBER(S)
AFRL-OSR-VA-TR-2012-0950

12. DISTRIBUTION/AVAILABILITY STATEMENT
Unlimited

Distribution A: Approved for Public Release

13. SUPPLEMENTARY NOTES

14. ABSTRACT
This research addresses theoretical and computational issues for estimation of gas concentration associated with an emitting stationary or moving source. Estimation of the concentration field provides a superior ability for detection of the gas source location, assessment of possible impacts and eventual containment. The model based concentration estimation is made possible via a sensing aerial vehicle (SAV). The theoretical component considers an abstract and finite-dimensional approximation framework that strongly couples theoretical estimation and control with advanced computational fluid dynamics methods. The gas dispersion model is based on the 2D advection diffusion equation with variable eddy diffusivities and ambient winds. The process state estimator is based on a 2D adaptive, multi grid, multi step finite volume method with upwind and flux limiting. The grid is adapted with local refinement and coarsening during the process state estimation, in order to improve accuracy and efficiency. The SAV motion dynamics is incorporated into the spatial process and its guidance is linked to the performance of the state estimator.

15. SUBJECT TERMS
State estimation; mobile sensors; grid adaptation; plume dispersion; source tracking.

16. SECURITY CLASSIFICATION OF:			17. LIMITATION OF ABSTRACT	18. NUMBER OF PAGES	19a. NAME OF RESPONSIBLE PERSON
a. REPORT	b. ABSTRACT	c. THIS PAGE			Michael A. Demetriou
Unlimited	Unlimited	Unlimited	Unlimited	35	19b. TELEPHONE NUMBER *(Include area code)* 508-831-5459

Summary

The dispersion of a plume from a stationary or moving gas source into an environment is representative of accidental or deliberate release of gases from land- or aerial-based vehicles, release of biochemicals, or the release of odors from biological systems. Dispersion can be modeled by advection-diffusion PDEs with spatially and time varying ambient mean velocity and eddy diffusivities. While mobile sensor-centric schemes for gas source detection can adequately perform for dispersion processes with constant wind and diffusivities, they are not applicable to processes with spatiotemporally varying wind and/or diffusivities. The model-based detection scheme incorporates the moving sensor location into the state-space formulation of the dispersion process and thus, can perform under general dispersion conditions. Moreover, the increase in computational power and efficiency in data acquisition hardware, enable the implementation of the model-based detection scheme onto a Sensing Aerial Vehicle (SAV). The development of a model-based detection scheme constitutes the main areas of this research effort.

The goals of research performed under FA9550-09-1-0469 were to:

- Develop a model-based estimation that provides the sensors position employed to find the proximity of the moving source. The sensor spatial relocation is accomplished by means of an SAV that has navigation and communication capabilities. The emphasis of the effort is on arriving at a model-based, optimal sensor repositioning during the search.

- Develop a finite-volume computational method on unstructured grids, that provides in realtime the solution (process-state estimate) of the 2D advection-diffusion PDE with variable diffusivities and ambient wind. The unstructured grid allows modeling of complex boundaries (e.g. objects) and will be adapted with local refinement and coarsening during the process-state estimation, in order to improve accuracy and efficiency.

The objectives of research performed under FA9550-09-1-0469 were to:

- Develop a new theoretical and approximating framework for the simultaneous estimation of the source location and the process state associated with a stationary or moving gas source that emits gases in an ambient environment.

- Develop a performance-based guidance of the sensing aerial vehicle.

- Develop and implement a computational method that provides in real-time the solution (process-state estimate) of the generalized PDE that models the 2D advection-diffusion process with variable diffusivities and ambient wind.
- Theoretical implementation of the proposed scheme is accomplished via an SAV that provides the spatial relocation of the sensor and communicates with a land-based station.

The Mathematical and Computational Accomplishments of the estimation approach are:

1. Examined various guidance schemes for the sensing aerial vehicle carrying the sensors.
2. Examined both kinematic and dynamic equations of motion for the guidance of the sensing aerial vehicle.

The Theoretical Accomplishments of the estimation approach are:

1. Developed a model-based estimation scheme that provides in real time the estimate of the concentration due to the gaseous release.
2. Provided an estimate of the proximity of the moving gaseous source via the motion of the mobile sensing aerial vehicle.
3. Developed a vehicle guidance scheme using Lyapunov redesign methods.
4. Incorporated the motion of the sensing aerial vehicle into the estimation equations.
5. Dictated the motion of the sensing aerial vehicle by the performance of the estimation scheme

The Computational Accomplishments of the computational method are:

1. Developed a multi grid, multi step finite volume method with upwind and flux limiting.
2. Developed grid adaptation with local refinement and coarsening during the process state estimation.

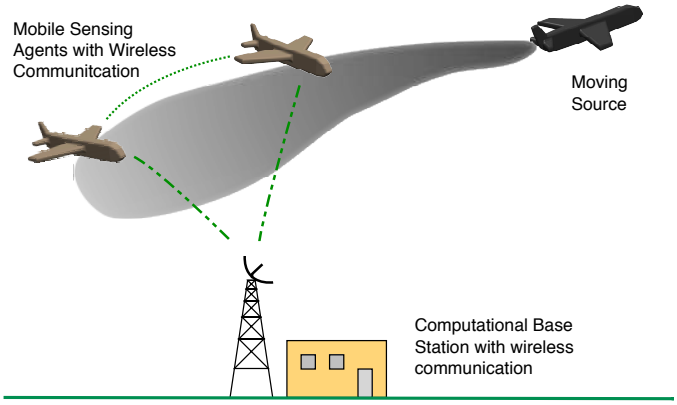

Figure 1: Overview of model-based estimation scheme with sensing aerial vehicles.

1 Overview

The goal of the work is to provide, in real time, an estimate of the gas concentration associated with an emitting moving source. Minimizing the damage from a toxic release must address not only the source location or its proximity, but also the contaminated material that has already been released (i.e. estimate the concentration field). The strategy applied in this research effort is not to reposition the sensors to areas of higher concentration (i.e. a local maximum concentration), but to send the sensors to areas of higher state estimation error. An overview of the proposed scheme is presented in Figure 1.

2 Physical model

The physical model employed for the estimation theory developed under FA9550-09-1-0469 is briefly described. The gaseous release under investigation is assumed to occur on a 2D plane given by $\Omega = [0, L_X] \times [0, L_Y] \subset \mathbb{R}^2$ which is assumed to be oriented parallel to the surface of the earth [1, 2, 3]. A moving point source $S(t, X, Y) = b(X, Y)u(t)$ is considered, having a release rate $u(t)$ and a spatial distribution $b(X, Y)$ with the spatial variables $(X, Y) \in \Omega$ and represented as

$$b(X, Y) = \delta(X - X_c(t))\delta(Y - Y_c(t)), \qquad (X, Y), (X_c(t), Y_c(t)) \in \Omega, \;\; t \in \mathbb{R}^+ \tag{1}$$

where the time varying centroid of the source is denoted by $\theta_c(t) = (X_c(t), Y_c(t)) \in \Omega$ [4, 5]. It is assumed that the dispersion of the gas is in the turbulent diffusion regime, that there are no chemical reactions,

the ambient speed (wind) is constant, and that there is no impact on the incompressible background. Under these conditions the dispersion can be described by the 2D advection-diffusion equation for the mean concentration $c(t, X, Y)$ given by [1, 2, 3]

$$\frac{\partial c}{\partial t} + W_X \frac{\partial c}{\partial X} + W_Y \frac{\partial c}{\partial Y} = \frac{\partial}{\partial X}\left(K_{XX}\frac{\partial c}{\partial X}\right) + \frac{\partial}{\partial Y}\left(K_{YY}\frac{\partial c}{\partial Y}\right) + S(t, \theta_c),$$
$$c\left(0, X, Y\right) = c_0\left(X, Y\right), \qquad (X, Y) \in \Omega, \;\; t \in \mathbb{R}^+$$

where W_X, W_Y are the mean (wind) speed of the background, and K_X, K_Y are the eddy diffusivities in the X and Y directions respectively. The resulting equation with the Dirichlet boundary conditions and unknown initial conditions is expressed as

$$\begin{aligned} &\frac{\partial c}{\partial t} + W_X \frac{\partial c}{\partial X} + W_Y \frac{\partial c}{\partial Y} = K_{XX}\frac{\partial^2 c}{\partial X^2} + K_{YY}\frac{\partial^2 c}{\partial Y^2} + S\left(t, \theta_c\right), \\ &c\left(0, X, Y\right) = c_0\left(X, Y\right), \;\; c\left(t, 0, 0\right) = c\left(t, L_X, 0\right) = c\left(t, 0, L_Y\right) = c\left(t, L_X, L_Y\right) = 0. \end{aligned} \tag{2}$$

3 Plant data generation

In the absence of measurements taken with the SAV, the sensor data (i.e. the plant) must be generated using (2). The numerical solution of (2) is obtained with a finite-volume method (FVM) [6]. The basic steps of this method are summarized following the implementation outlined in Gatsonis *et al.* [7]. The computational domain Ω is discretized with a set of $(N_X+1)\times(N_Y+1)$ grid points defining the centers of $N = N_X \times N_Y$ rectangular finite volumes. The PDE (2) is written in conservative form as

$$\frac{\partial c}{\partial t} + \frac{\partial (cW_X)}{\partial X} + \frac{\partial (cW_Y)}{\partial Y} - \frac{\partial}{\partial X}\left(K_X \frac{\partial c}{\partial X}\right) - \frac{\partial}{\partial y}\left(K_Y \frac{\partial c}{\partial Y}\right) = S(t, \theta_c). \tag{3}$$

This flux-form is integrated over a fixed finite volume Ω_c with a surface area $\mathbf{A} = A\hat{\mathbf{n}}$ as

$$\frac{\partial}{\partial t}\iint\limits_{\Omega} c dV + \oint\limits_{S} \mathbf{F}\cdot\mathbf{n} dS = \iint\limits_{\Omega} S dV, \tag{4}$$

where the total flux term is expressed as the sum of the convective and diffusive terms

$$\mathbf{F} = \left(f_X^C + f_X^D\right)\hat{\mathbf{X}} + \left(f_Y^C + f_Y^D\right)\hat{\mathbf{Y}},$$

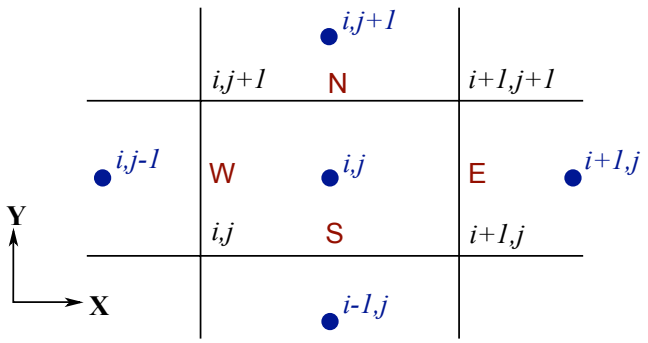

Figure 2: Graphical representation of the state error for guidance scheme.

with

$$f_X^C = cW_X, \quad f_Y^C = cW_Y \quad f_X^D = -K_{XX}\frac{\partial c}{\partial X}, \quad f_Y^D = -K_{YY}\frac{\partial c}{\partial Y}.$$

The integration (4) over a cell volume $\Omega_{c,ij}$ with vertex (ij) shown in Figure 2 results in the semi-discrete equation

$$dc_{ij}/dt = -1/\Omega_{c,ij}\sum_{sides}\left(\mathbf{F}_{ij}^E.\mathbf{A}_{ij}^E + \mathbf{F}_{ijk}^W.\mathbf{A}_{ijk}^W + \mathbf{F}_{ij}^N.\mathbf{A}_{ij}^N + \mathbf{F}_{ijk}^S.\mathbf{A}_{ijk}^S\right) + S_{i,j}. \tag{5}$$

The flux evaluation requires in general the local normal to a surface. For example, on the east surface of the volume (ij) the normal is

$$n_{ij}^E = n_{X,ij}^E\hat{\mathbf{X}} + n_{Y,ij}^E\hat{\mathbf{Y}},$$

and the flux is

$$\mathbf{F}_{ij}^E\mathbf{A}_{ij}^E = (f_{ij}^{CE} + f_{ij}^{DE})n_{X,ij}^E A_{ij}^E + (g_{ij}^{DE} + g_{ij}^{DE})n_{Y,ij}^E A_{ij}^E.$$

For the structured grid with rectangular finite volumes considered here, the local normal is positive away from each finite volume surface

$$\mathbf{n}_{ij}^E = \hat{\mathbf{X}}, \quad \mathbf{n}_{ij}^W = -\hat{\mathbf{X}}, \quad \mathbf{n}_{ij}^B = \hat{\mathbf{Y}}, \quad \mathbf{n}_{ij}^S = -\hat{\mathbf{Y}},$$

$$\mathbf{F}_{ijk}^E.\mathbf{A}_{ijk}^E = (f_{ijk}^{CE} + f_{ijk}^{DE})A_{ijk}^E.$$

The convective flux f_{ij}^{CE} at the east boundary is calculated as the average of cell centered fluxes for adjacent cells as

$$f_{ij}^{CE} = \frac{1}{2}\left(f_{i+1,j}^{CE} + f_{ij}^{CE}\right).$$

The diffusive flux for the east boundary is calculated with a central difference approach at the cell interface as

$$f_{ij}^{DE} = K_{XX}\left.\frac{\partial c}{\partial X}\right|_{i,j}^{E} = K_{XX}|_{ij}\frac{c_{i+1,j} - c_{i,j}}{X_{i+1,j} - X_{i,j}}.$$

The flux calculation for the remaining three sides follows similarly. The cell Péclet number is a measure of the relative strengths of the convective and diffusive parts of the flow and is defined as $Pe = W/K$. At larger Péclet numbers ($|Pe| > 2$), the convective fluxes are evaluated using upwinding. For $W_X > 0$,

$$f_{ij}^{CE} = f_{ij}^{CE} = cW_X|_{ij}, \quad f_{ij}^{CW} = f_{i-1,j}^{CW} = cW_X|_{i-1,j}.$$

For $W_X < 0$,

$$f_{ij}^{CE} = f_{i+1,j}^{CE} = cW_X|_{i+1,j}, \quad f_{ij}^{CW} = f_{ij}^{CW} = cW_X|_{ij}.$$

The semi-discrete equation (5) can be written as

$$dc_{ij}/dt = -1/\Omega_{ij}\ \left[c_{i+1,j}a_{ij}^{E} + c_{i-1,j}a_{ij}^{W}c_{i,j+1}a_{ij}^{N} + c_{i,j-1}a_{ij}^{S} + c_{i,j}a_{ij}^{P}\right] + S_{i,j}. \tag{6}$$

The coefficients are given by

$$a_{ij}^{W} = \max\left[F_W, \left(D_W + \frac{F_W}{2}\right), 0\right],\ a_{ij}^{E} = \max\left[-F_E, \left(D_E - \frac{F_E}{2}\right), 0\right],$$

and D_W, D_E, F_W and F_E are defined as

$$D_W = \frac{K_W}{\delta X_{WP}}\mathrm{A}_W,\ \ D_E = \frac{K_E}{\delta X_{PE}}\mathrm{A}_E,\ \ F_W = (cW_X)_W\,\mathrm{A}_W,\ \ F_E = (cE_X)_E\,\mathrm{A}_E.$$

where δX_{WP} is the distance between the volume (ij) and the west volume. Application of (6) to all cell centers, leads to a system of $(N_X \times N_Y) = N$ semi-discrete ODEs.

Introducing $\mathbf{x} = \mathbf{c} = \{c_1, \ldots, c_N\}$ as the finite dimensional representation of the state vector, the

indexing for mapping from (ij) to n is expressed as

$$c_n = c_{ij}, \;\; n = (j-1)N_X + i, \;\; j = 1, N_Y, \;\; i = 1, N_X.$$

The system of semidiscrete ODEs can then be written in the state-space form as

$$\dot{\mathbf{x}} = A\mathbf{x} + Bu. \tag{7}$$

The source is represented by the release rate $u\,(t)$ and the spatial distribution associated with the source location (X_c, Y_c), (1). For a point source release located within volume (ij), the vector B is all zeros with a 1 located at $B\,(n)$. The $(N \times N)$ state matrix A is associated with the finite dimensional approximation of the advection diffusion equation. The operator $A\,(t)$ is constructed with the a coefficients. The a_P coefficient located at $A\,(n, n)$ is the entry for the nth finite volume and thus the entry for the corresponding state $\mathbf{x}_n$. The remaining coefficient are located at $A\,(n, m)$, where m is the index location of the corresponding neighboring node.

The system of semi-discrete ODE's as in equation (5) is integrated using the four-step Runge-Kutta scheme expressed as

$$c^{(m)} = c^{(n)} - \alpha_m \Delta t R^{(AV)} c^{(m-1)}, \quad m = 1, 2, 3, 4, \quad c^{(n+1)} = c^{(4)}$$

where $c^{(n)}$ is the concentration at time level n and $\alpha_1 = 0.25$, $\alpha_2 = 0.333$, $\alpha_3 = 0.5$, $\alpha_4 = 1.0$.

3.1 Sensor measurements from numerically generated process model

The sensor is assumed to have measurement data on the concentration and gradient at its current spatial location. Measurement data is taken from the simulation of the plant. The state measurement at the spatial location, $c(X, Y)$, is calculated as the weighted average based on the inverse distance to the 4 nearest volume centers

$$c(X, Y) = \frac{c_{NE} * d_{NE}^{-1} + c_{SE} * d_{SE}^{-1} + c_{SW} * d_{SW}^{-1} + c_{NW} * d_{NW}^{-1}}{d_{NE}^{-1} + d_{SE}^{-1} + d_{SW}^{-1} + d_{NW}^{-1}}.$$

The structured discretization of the grid allows the local gradient $(\frac{\partial c}{\partial X}, \frac{\partial c}{\partial Y})$ to be calculated with the second order central differencing scheme for nonuniform spacing [6, 8]. This approach calculates the gradient based

on two computational points in each direction and the distance to the points.

4 Model-based State Estimation and Sensor Guidance

4.1 Output measurement model

Numerous sensors are available for the measurement of trace species in the atmosphere. They are available in several types with many different operating characteristics including size, sensitivity, dynamic range, reliability, and response time [9, 10, 11, 12]. Here, a specific sensor and contaminant pair have not been chosen, so a generalized sensor model is constructed based on realistic sensor parameters. It is assumed that the sensor is selective and able to distinguish the contaminant from the other constituents in the atmosphere.

A mobile agent equipped with a sensor is able to provide concentration information $c(t, X, Y)$ at the spatial point $\theta_s = (X_s, Y_s) \in \Omega$. Similar to the source model in (1), the spatial distribution of the sensor is also modeled by a spatial Dirac delta function. It is assumed that there is no noise and the measurement device provides exact readings of the local concentration

$$y(t; \theta_s) = c(t, X_s, Y_s) = \int_0^{L_X} \int_0^{L_Y} \delta(X - X_s)\delta(Y - Y_s)c(t, X, Y)\, dX\, dY$$

With the sensor mounted on a mobile agent (SAV), it is able to provide measurement data at various locations within the spatial domain Ω as a function of time. The time dependent sensor measurement taken at the centroid $\theta_s(t)$ of the sensor is then

$$y(t; \theta_s(t)) = \int_0^{L_X} \int_0^{L_Y} \delta(X - X_s(t))\delta(Y - Y_s(t))c(t, X, Y)\, dX\, dY. \tag{8}$$

which is essentially the concentration $c(t, X, Y)$ at the current position $\theta_s(t)$ of the SAV.

4.2 Abstract formulation of advection diffusion PDE

The advection diffusion PDE (2) can be viewed as an evolution equation in an appropriate Hilbert space. Such an abstract formulation is conducive to both the ensuing stability analysis for the resulting state estimator and its finite dimensional approximation.

The state space is taken to be $\mathcal{X} = L^2(\Omega)$ equipped with inner product denoted by $\langle \cdot, \cdot \rangle$ and norm by

$|\cdot|$. Additionally, we consider $\mathcal{V} = H_0^1(\Omega)$ be the Sobolev space with $\mathcal{V}$ dense in $\mathcal{X}$. Such a consideration is necessitated as the output and input operators are defined in $\mathcal{V}$ and its dual $\mathcal{V}^*$ [13]. The concentration state is an element of the Hilbert space $x(t) = c(t, \cdot, \cdot)$ in $\mathcal{X}$ over $[0, T]$. The PDE (2) can then be written as an evolution equation [14, 15]

$$\begin{aligned} \dot{x}(t) &= \mathcal{A}x(t) + \mathcal{B}(\theta_c(t))u(t), \quad x(0) = x_0 \in \mathcal{X} \\ y(t; \theta_s(t)) &= \mathcal{C}(\theta_s(t))x(t) \end{aligned} \tag{9}$$

where $\mathcal{A} \in \mathcal{L}(\mathcal{V}, \mathcal{V}^*)$ is the elliptic operator associated with the advection diffusion PDE (2), $\mathcal{B}(\theta_c(t))$ is the location-parameterized input operator associated with the source spatial distribution $b(X, Y)$ in (1), and $\mathcal{C}(\theta_s(t))$ is the output operator associated with the time dependent sensor measurement (8). For the problem to be well posed, one needs to impose $\mathcal{B}(\theta_c(\cdot))f(\cdot) \in L^2(0, T; \mathcal{V}^*)$, see [16, 17, 15]. Equation (7), as used for plant generation, constitutes a finite dimensional representation of the evolution equation (9).

4.3 Model-based State estimation

The estimator developed in [18] is modified to account for vehicle dynamics and is applied in this work to estimate the concentration state over the entire spatial domain. In summary, a Luenberger observer is implemented with the filter gain taken to be a constant multiple of the dual of the output operator (collocated) and given by

$$\dot{\widehat{x}}(t) = \Big(\mathcal{A} - \gamma \mathcal{C}^*(\theta_s(t))\mathcal{C}(\theta_s(t))\Big)\widehat{x}(t) + \gamma \mathcal{C}^*(\theta_s(t))y(t; \theta_s(t)), \quad \widehat{x}(0) \neq x(0), \;\; \gamma > 0, \tag{10}$$

Equation (10) constitutes half of the integrated estimation and guidance equations. It is accompanied by another equation that provides the time-variation of the sensor centroid $\theta_s(t)$, which would dictate the spatial repositioning of the SAV within the spatial domain Ω. This spatial repositioning is given implicitly in terms of the control inputs (torques) to the aerial vehicles that carries the sensor.

Sensor guidance is dependent on the state estimation error, that is $\mathbf{e}(t) = x(t) - \widehat{x}(t)$. The spatially distributed state error $e(t, X, Y) = x(t, X, Y) - \widehat{x}(t, X, Y)$ may be denoted simply as $\mathbf{e}(t)$ when considered

as an element of the Hilbert space $\mathcal{X}$. Using (9) and (10), the evolution of the state error is

$$\begin{aligned} \dot{\mathbf{e}}(t) &= \mathcal{A}(\theta_s(t))\mathbf{e}(t) + \mathcal{B}(\theta_c(t))u(t), \\ \mathbf{e}(0) &= \mathbf{e}_0 \in \mathcal{X}. \end{aligned} \tag{11}$$

where $\mathcal{A}_{cl}(\theta_s(t)) \triangleq \Big(\mathcal{A} - \gamma \mathcal{C}^*(\theta_s(t))\mathcal{C}(\theta_s(t))\Big)$.

4.4 Sensing device model

The physical construction of sensors introduces inherent limitations in the sensor operation. Ram et al [9] provide a good discussion on sensor construction and design. Many trace contaminant sensors do not take continuous measurements, but instead have a recovery time or transient response time between sensor readings [10, 19, 20]. Transient effects limit the time between accurate sensor readings. A sensor that provides accurate measurements at a very fast sample rate will clearly provide more information than one that samples slower. This research effort is interested in real time state estimation, so faster measurement frequencies are desirable. Optical based sensors such as chemiluminescence detectors and absorption spectroscopy are able to sample every 1-5 seconds [10]. For the numerical experiment considered in this research effort, time between samples is taken to be 2 seconds.

Sensor dead-zone and threshold saturation are also implemented in the model. All trace contaminant sensors have maximum and minimum sensing thresholds that determine the limits of the sensing ability. When the state is below a minimum threshold c_{min}, the sensing device does not detect an elevated measurement. This is referred to as a dead-zone. When the state is above the maximum c_{max}, the output from the sensor is the saturated value. These limits are expressed below

$$c_S(X_s, Y_s) = \begin{cases} 0 & c(X_s, Y_s) < c_{min} \\ c(X_s, Y_s) & c_{min} < c(X_s, Y_s) < c_{max} \\ c_{max} & c(X_s, Y_s) > c_{max} \end{cases} \tag{12}$$

When taking sensor measurements on the environment, the time rate of change of the sensor depends on the process under investigation (the atmospheric advection diffusion) as well as the motion of the sensor

and the spatial gradient of the concentration [21] as shown below

$$\frac{dc}{dt} = \left(\frac{\partial c}{\partial t}\right)_{X,Y} + \frac{dX}{dt}\left(\frac{\partial c}{\partial X}\right)_{Y,t} + \frac{dY}{dt}\left(\frac{\partial c}{\partial Y}\right)_{X,t}$$

where $\frac{dX}{dt}$ is the velocity of the sensor in the X direction and $\frac{\partial c}{\partial X}$ is the spatial gradient of the contaminant in the X direction. This effort simplified sensor measurements and assumed sensor readings at the current location of the sensing agent were directly available.

4.5 SAV dynamics

The movement of the sensor throughout the domain is accomplished with an SAV. For simplicity, the sensor location is taken to be at the barycenter of the SAV. The equations of motion describing the mobile agent position will then be valid for the position of the sensor centroid.

Depending on the focus of the work, mobile agents may be modeled with great detail [22, 23] or very simply [24, 25, 26, 27]. In this effort, the mobile agent is modeled as a fixed wing unmanned aerial vehicle with basic autopilot controls. With knowledge of its own state, the lower level controllers account for deviations in the trajectory of the aircraft caused by wind, coupled control surfaces, and other disturbances. The SAV is assumed to be rigid and symmetric with a collocated center of mass and center of gravity, which allows the equation of motion to be presented in a more compact form. The mass and moment of inertia are assumed constant throughout the simulation. For simplicity, many works focus on the kinematic motion and neglect the dynamics. However,, in order to provide a more accurate representation of the SAV motion, this research effort considered the dynamic equations of motion.

The SAV motion is constrained due to the physical limitations of the aircraft. The agent's speed, $v(t)$, and turning rate, $\omega_\psi(t)$, are constrained within maximum and minimum values [27, 28, 29].

$$0 < v_{min} \leq v \leq v_{max}, \qquad -\omega_{\psi_{max}} \leq \omega_\psi \leq \omega_{\psi_{max}}.$$

The thrust and turning force are also constrained as

$$-\tau_{l_{max}} \leq \tau_l \leq \tau_{l_{max}}, \qquad -\tau_{amax} \leq \tau_a \leq \tau_{amax}.$$

For an aircraft equipped with a lower level autopilot [29, 23], the pose of the sensor may be described

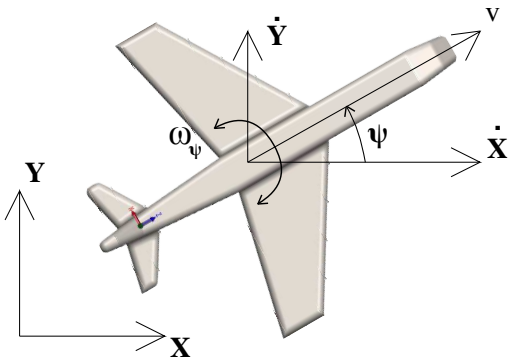

Figure 3: Schematic of the SAV coordinate system in 2D.

by the kinematic equations [27] given by

$$\dot{X}(t) = v(t)\cos(\psi(t)), \qquad \dot{Y}(t) = v(t)\sin(\psi(t)), \qquad \dot{\psi}(t) = \omega_{\psi}(t), \tag{13}$$

where the pose is represented by the cartesian position (X, Y) and the SAV's heading angle ψ. The motion is determined by the SAV's speed and angular turning rate $(v(t), \omega_{\psi}(t))$ as shown in Figure 3. Equation (13) can be expressed in matrix form

$$\dot{\mathbf{q}}(t) = \mathbf{S}(t)\mathbf{v}(t) \tag{14}$$

where $\dot{\mathbf{q}}(t) = \left[\dot{X}(t), \dot{Y}(t), \dot{\psi}(t)\right]^T$, $\mathbf{v}(t) = \left[v(t), \dot{\psi}(t)\right]^T$, and the transformation matrix $\mathbf{S}(t)$ is

$$\mathbf{S}(t) = \begin{bmatrix} \cos(\psi) & 0 \\ \sin(\psi) & 0 \\ 0 & 1 \end{bmatrix}. \tag{15}$$

These equations are the same for those of a differential drive robot [29], with the additional constraint that the fixed wing aircraft must hold a minimum forward velocity to maintain lift.

The 2D dynamic equations of motion for steady state flight given in inertial coordinates [30, 31, 24, 25,

23] are given by

$$\mathcal{M}\begin{bmatrix} \ddot{X} \\ \ddot{Y} \\ \ddot{\psi} \end{bmatrix} = \begin{bmatrix} \cos(\psi) & 0 \\ \sin(\psi) & 0 \\ 0 & 1 \end{bmatrix} \begin{bmatrix} \tau_l \\ \tau_a \end{bmatrix} + \begin{bmatrix} -M\dot{\psi}vsin\psi \\ M\dot{\psi}vcos\psi \\ 0 \end{bmatrix} \tag{16}$$

where τ_l is the *thrust* and τ_a is the *angular torque* applied by the control surfaces to the center of mass. Since the equations are for steady flight, there is no explicit drag component. With τ_l and τ_a set to zero, the aircraft maintains constant speed and angular turning rate. The mass matrix $\mathcal{M}$ is expressed as $\mathcal{M} = \text{diag}\{M, M, I\}$, where M is the mass and I the moment of inertia of the SAV. Equation (16) can be rewritten in matrix form as

$$\mathcal{M}\ddot{\mathbf{q}} = \mathcal{B}_1\tau - \mathbf{A}^T\lambda. \tag{17}$$

Substituting equation (14) into equation (17), along with $\dot{\mathbf{q}} = \dot{\mathbf{S}}\mathbf{v} + \mathbf{S}\dot{\mathbf{v}}$, result in

$$\mathcal{M}(\dot{\mathbf{Sv}}) = \mathcal{B}_1\tau - \mathbf{A}^T\lambda \Rightarrow \mathcal{M}\mathbf{S}\dot{\mathbf{v}} + \mathcal{M}\dot{\mathbf{S}}\mathbf{v} = \mathcal{B}_1\tau - \mathbf{A}^T\lambda.$$

Premultiplying by $\mathbf{S}^T$ yields

$$\mathbf{S}^T\mathcal{M}\mathbf{S}\dot{\mathbf{v}} + \mathbf{S}^T\mathcal{M}\dot{\mathbf{S}}\mathbf{v} = \mathbf{S}^T\mathcal{B}_1\tau - \mathbf{S}^T\mathbf{A}^T\lambda. \tag{18}$$

The equation is simplified with the introduction of the transformed mass matrix $\mathcal{M}_1 = \mathbf{S}^T\mathcal{M}\mathbf{S} = \text{diag}\{M, I\}$. The term $\mathbf{S}^T\mathcal{M}_1\dot{\mathbf{S}}$ is simplified to $\mathbf{S}^T\mathcal{M}_1\dot{\mathbf{S}} = \mathbf{0}_{2\times1}$. The input control matrix $\mathcal{B}_2$ is also simplified to $\mathcal{B}_2 = \mathbf{S}^T\mathcal{B}_1 = \mathbf{I}_{2\times2}$. As a consequence of the premultiplication by $\mathbf{S}^T$, the constraint matrix is eliminated from (17) since $\mathbf{S}^T\mathbf{A}\lambda = \mathbf{0}_{2\times1}$. For the inputs $\tau = [\tau_l, \tau_a]$, the dynamic equation of motion from (18) can then be written as

$$\mathcal{M}_1\dot{\mathbf{v}} = \mathcal{B}_2\tau. \tag{19}$$

Remark 1 *When the SAV is assumed massless and inertialess, the kinematic equations* (14) *can be used to describe the SAV motion in 2D. If it is further assumed that its motion is holonomic and not constrained by* (14)*, then it is able to implement motion with any desired direction and speed. In fact, this was considered in [18].*

4.6 SAV guidance

The Lyapunov functional used in [18, 32, 33] is modified to include the kinetic energy of the SAV

$$V = -\langle \mathbf{e}(t), \mathcal{A}_{cl}(\theta_s(t))\mathbf{e}(t)\rangle + KE.$$

The kinetic energy of SAV is related to its mass and velocity as $KE = \frac{1}{2}\dot{\mathbf{q}}^T\mathcal{M}\dot{\mathbf{q}}$. Transforming from cartesian velocities to body velocities with equation (14) yields $KE = \frac{1}{2}\mathbf{v}^T\mathbf{S}^T\mathcal{M}\mathbf{S}\mathbf{v} = \frac{1}{2}\mathbf{v}^T\mathcal{M}_1\mathbf{v}$. For an aircraft with its motion constrained in a 2D plane parallel to the ground, the gravitational potential energy term is equal to zero. The Lyapunov functional is re-written

$$V = -\langle \mathbf{e}, \mathcal{A}_{cl}(\theta_s)\mathbf{e}\rangle + \frac{1}{2}\mathbf{v}^T\mathcal{M}_1\mathbf{v} \tag{20}$$

Taking the time derivative of the Lyapunov functional along the trajectories of the state error (11) and the complete dynamics of the craft (14), (19) yields

$$\begin{aligned}\dot{V} &= \left(-|\mathcal{A}_{cl}(\theta_s)\mathbf{e}|^2 + \varepsilon\varepsilon_X\dot{X} + \varepsilon\varepsilon_Y\dot{Y}\right) + \mathbf{v}^T\mathcal{M}_1\dot{\mathbf{v}} \\ &= -|\mathcal{A}_{cl}(\theta_s)\mathbf{e}|^2 + \begin{bmatrix} \varepsilon\varepsilon_X & \varepsilon\varepsilon_Y & 0 \end{bmatrix}\dot{\mathbf{q}} + \mathbf{v}^T\mathcal{M}_1\dot{\mathbf{v}}.\end{aligned}$$

Substituting equations (14) and (19) simplifies to

$$\begin{aligned}\dot{V} &= -|\mathcal{A}_{cl}(\theta_s)\mathbf{e}|^2 + \begin{bmatrix} \varepsilon\varepsilon_X & \varepsilon\varepsilon_Y & 0 \end{bmatrix}\mathbf{S}\mathbf{v} + \mathbf{v}^T\mathcal{M}_1\dot{\mathbf{v}} \\ &= -|\mathcal{A}_{cl}(\theta_s)\mathbf{e}|^2 + \begin{bmatrix} \varepsilon\varepsilon_X & \varepsilon\varepsilon_Y & 0 \end{bmatrix}\mathbf{S}\mathbf{v} + \mathbf{v}^T\mathcal{B}_2\tau,\end{aligned} \tag{21}$$

where ε denotes the state estimation error at the current sensor location and $\varepsilon_X, \varepsilon_Y$ denote the spatial gradients of the estimation error at the sensor location. The control law can now be developed to ensure that the Lyapunov derivative is negative semi-definite and the guidance scheme drives the sensor to areas of higher state error. Focusing on the part of equation (21) to be made negative definite and recognizing that $\mathbf{v}^T\mathcal{B}_2\tau = \left(\mathbf{v}^T\mathcal{B}_2\tau\right)^T$ gives

$$\begin{bmatrix} \varepsilon\varepsilon_X & \varepsilon\varepsilon_Y & 0 \end{bmatrix}\mathbf{S}\mathbf{v} + \left(\mathcal{B}_2\tau\right)^T\mathbf{v} \leq 0$$

Solving for the input torque yields the following control guidance law

$$\boxed{\tau = -\mathcal{B}_2^{-1}\mathbf{S}^T \begin{bmatrix} \varepsilon\varepsilon_X & \varepsilon\varepsilon_Y & 0 \end{bmatrix}^T} \tag{22}$$

To better understand the control law (22), the matrices are expanded as

$$\begin{bmatrix} \tau_l \\ \tau_a \end{bmatrix} = - \begin{bmatrix} \cos\psi & \sin\psi & 0 \\ 0 & 0 & 1 \end{bmatrix} \begin{bmatrix} \varepsilon\varepsilon_X \\ \varepsilon\varepsilon_Y \\ 0 \end{bmatrix} = \begin{bmatrix} -\varepsilon\varepsilon_X \cos\psi - \varepsilon\varepsilon_Y \sin\psi \\ 0 \end{bmatrix} \tag{23}$$

The above relates the SAV motion control, via the torque τ, to the performance of the estimator; in other words *the motion of SAV is dictated by the performance of the estimator and is given explicitly in terms of the output estimator error $\varepsilon(t)$ and the spatial gradients $\varepsilon_X(t), \varepsilon_Y(t)$ of the estimation error at the current sensor location.*

The control torque can further be modified to make $\dot{V} = -|\mathcal{A}_{cl}(\theta_s)\mathbf{e}|^2 - \mathbf{v}^T K \mathbf{v}$ "more" negative by including velocity terms

$$\begin{aligned} \tau_l &= -c_1(\varepsilon\varepsilon_X \cos\psi + \varepsilon\varepsilon_Y \sin\psi) - k_1 v - k_{12}\dot{\psi}, \qquad c_1 > 0,\ k_1 > 0, k_{12} \geq 0 \\ \tau_a &= -k_{12} v - k_2 \dot{\psi}, \qquad k_2 > 0, k_{12} \geq 0. \end{aligned} \tag{24}$$

The constants c_1, k_1, k_{12} are user-defined guidance gains, chosen to achieve desired sensor performance. In this research effort, c_1 was chosen so that the input torque is of the same order of magnitude as the agent physical limitations (i.e. the input is not always saturated). The $-k_1 v - k_{12}\dot{\psi}$ term was not required for this instance.

The Lyapunov-based guidance scheme (22) only provides motion control inputs for the thrust τ_l. While the extension in (24) could possibly include a velocity term in the rotational dynamics via the additional entries of the positive semi-definite matrix K

$$I\ddot{\psi} = \tau_a = -k_{12} v - k_2 \dot{\psi}, \qquad k_2 > 0, k_{12} \geq 0$$

it is nonetheless unable to address the rotational motion in an effective manner. A supplementary controller

was used whereby the angular torque input was given by

$$\tau_a(t) = I\ddot{\psi}^d(t) - k_d\left(\dot{\psi}^a(t) - \dot{\psi}^d(t)\right) - k_p\left(\psi^a(t) - \psi^d(t)\right) \tag{25}$$

The current heading angle was taken to be $\psi^a(t)$. The desired heading angle $\psi^d(t)$ was defined as the angle created by the two cartesian torques

$$\psi^d = \arctan\left(\frac{\epsilon_Y}{\epsilon_X}\right)$$

The above choice stems from the work in [18] which considered a massless and inertialess sensing agent. From equation (25), $\dot{\psi}^d$, the time derivative of the desired angle was calculated numerically.

4.7 SAV deployment model

Prior to initiating the tracking scheme, the SAV assumes no source is present in the domain. With knowledge of the current wind profile, the sensor is strategically placed downwind in the domain. As the wind blows, it will advect contaminant towards the sensor. Although patrolling downwind of the source will increase the probability of detecting a source in the domain, the search strategy is not assumed optimal. The sensor travels in a circular path downwind continuously taking readings until it detects an elevated concentration, (12). The sensing agent then stops patrolling and begins searching for the source via (10), (22), (25). At this point, the detection scheme begins estimating the process state and providing the mobile sensing agent with the appropriate command signals from the guidance scheme.

5 Finite dimensional approximation and sensor-based grid adaptation

The estimator is approximated as a finite dimensional system similar to the approach used with the plant in (7). A conservative form of the advection diffusion equation is used and integrated with the four stage Runge-Kutta scheme. Since it is desired to calculate the estimator in real time, the dimension of its finite dimensional approximation is reduced compared to that of the plant. To maintain a desired level of accuracy in regions of interest, while keeping the computational requirements, grid adaptation is implemented. The implementation of a reduced dimensional estimator also avoids the *inverse crime* problem that is associated with a numerical simulation and inversion that are of the same discretization. An equivalent discretization in the forward simulation and estimated state would provide results that are overly optimistic [34].

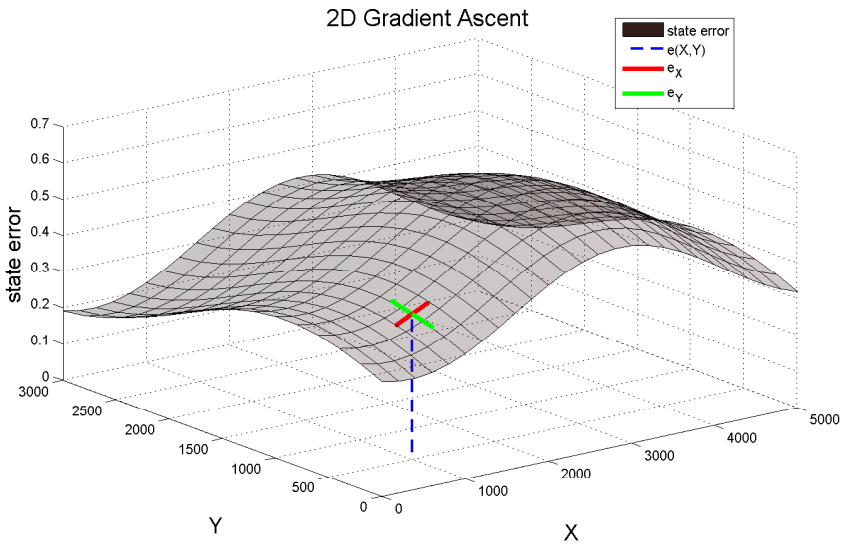

Figure 4: Graphical representation of the state error for guidance scheme.

The limited computation power and desire for a real time solution suggested the use of grid adaptation techniques [35, 36]. For this research effort, a combination of a stretched grid and switched system were implemented. The estimation scheme discretized the domain with 9 stretched grids. Each of the stretched grids consisted of a predefined number of volumes in each direction. This created a system that was low enough in dimension to be solved in real time. Each stretched grid had an area of relatively high resolution that was meant to focus on the area of interest. The rest of the domain consisted of a coarser discretization to keep computational requirements low. Autonomous state dependent switching [37] control was applied. When the area of interest changed, the grid was switched to ensure the location of interest always had a higher degree of discretization than the rest of the domain.

This hybrid dynamical system couples the estimation scheme with the computational scheme, using one to enhance the other. Numerically, this switching changes several of the matrices used in the state space formulation. At each switching instance, the state matrix A had to be recalculated. The data from the old stretched grid was moved to the new one by means of a prolongation and restriction operation. A prolongation operator transferred information from the old grid to a new, higher dimensional one with higher resolution. A restriction operator then transferred the data to the new grid. Nine restriction and prolongation operators were created a priori in order to handle all switching cases [35]. This helped to minimize computations during the state estimation. The output C matrix changed just slightly due to the

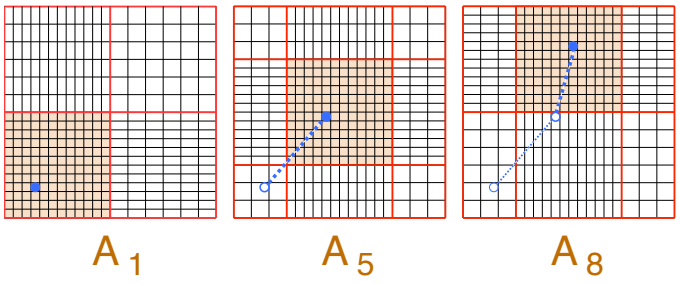

Figure 5: Example of grid adaptation with high resolution area highlighted.

spatial location of the sensor, but since it was created at each time step, information did not have to be transferred from one to another when the switch occurred. Below, Algorithm 1 outlines the grid adaptation logic. Figure 5 demonstrates the grid adapting from Grid 1, to Grid 5, then to Grid 8 as the sensor position moves between the locations noted. The set of available switched grids resulted in a family of matrices

Algorithm 1 State dependent grid adaptation

```
estimate (X, Y, ψ)_c
calculate nearest switched grid
if nearest grid ≠ current grid then
    set new grid to nearest grid
    switch state matrix, A
    prolongate concentration data to general grid
    restrict state information to new grid
end if
```

$\{A_i,\, i \in \mathcal{I}\}$ based on the index set $\mathcal{I}$. In this research effort, the switching signal (which was based on the sensor location) was a piecewise constant function in time represented by $\sigma : [0, \infty) \to \mathcal{I}$. Consider the family $(S_p)_{p\in\mathcal{I}}$ of linear systems that are continuous in time. For each $p \in \mathcal{I}$, the estimator is given by

$$\dot{\widehat{x}}^n(t) = \left(A_p - \gamma C_p^T(\theta_s(t))C_p(\theta_s(t))\right)\widehat{x}^n(t) + \gamma C_p^T(\theta_s(t))y(t;\theta_s(t)) \tag{26}$$

The current sensor position $\theta_s(t)$ dictates the switching signal and subsequently the choice of the matrices A_p, C_p. At the same time, the state estimator along with the guidance scheme (10), (22) provide the spatial repositioning of the SAV.

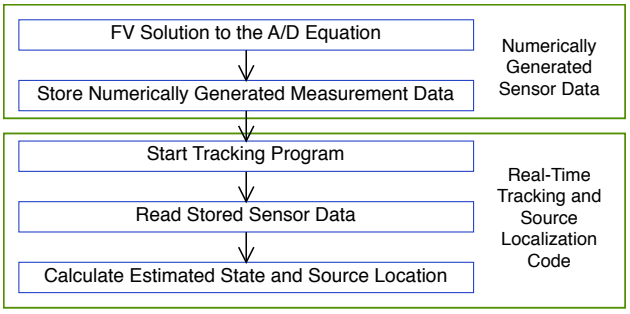

Figure 6: Simulation Flow Chart.

6 Implementation pseudo code and flowchart

Due to the lack of experimental data, simulations for this work were carried out in two parts. The first part consisted of generating acceptable sensor data that the estimator could access in place of real measurements as described in Section 3. A source in a 2D domain was simulated on a high dimensional system with the concentration profile saved to file at every time step. The high dimensional approximation was computationally expensive and was therefore done a priori and stored to file. In practice, this step would not be required and measurement data would be taken directly. The pseudocode for the generation of experimental data can be seen in Algorithm 2. The actual estimation was done in the second part of the simulation. As the sensing

Algorithm 2 Generating of Sensor Data

1: **read** simulation parameters
2: discretize high dimensional uniform grid
3: **for** $t = dt$ to t_{final} **do**
4: calculate source location $(X, Y)_c$
5: RK4 integration of forward state x
6: apply boundary conditions
7: **end for**
8: **output** state at each time step to file

aerial vehicle moved around the spatial domain, it was continuously taking measurements, which consisted of reading small portions of the stored data from the files created in the generation of source data. Algorithm 3 details the estimation process and the entire simulation is outlined in Figure 6.

Algorithm 3 State Estimation Scheme

Require: Output data files from forward problem.

read simulation parameters
generate a priori switched system grids
known $(X, Y, \psi)_s$
for $t = dt$ to t_{final} **do**
  read $c(X_s, Y_s, t)$, $\frac{\partial c(X_s,Y_s,t)}{\partial X}$, $\frac{\partial c(X_s,Y_s,t)}{\partial Y}$
  if $c(X, Y, \psi) \geq y_{min}$ **then**
    if request command signal **then**
      $\tau_l(t) \leftarrow -c_1(\varepsilon\varepsilon_X \cos\psi + \varepsilon\varepsilon_Y \sin\psi) - k_1 v - k_{12}\dot{\psi}$
      $\tau_a(t)$ from (25)
    end if
    RK4 integration of $\hat{x}$
    apply BCs
  else
    continue patroling
  end if
  calculate new $(X, Y)_s$
  switch grid
end for

7 Summary of Simulation Results

Several simulations have been performed with the developed guidance scheme. For consistency, the domain size in each case was taken to be 4 km $\times$ 4 km. The eddy diffusivity was assumed constant in space and time as $20\text{m}^2/\text{s}$. The wind was also assumed constant in space and time, blowing at $5\text{m}/\text{s}$ to the East and $5\text{m}/\text{s}$ to the North. In all cases, the sensor started in the downwind area of the domain in a patrolling behavior. Simulations are conducted on a 5 node Linux cluster running Red Hat 3.4.6. The serial code was implanted on one of the nodes with a Quad Core Intel Xeon processor running at 2.33GHz and 16GB of RAM. The code was compiled with Intel's Fortran compiler IFORT version 9.0. Data visualization was performed with Tecplot 360 software version 12 running on a Windows 7 workstation.

The numerical discretization of the forward problem (plant) in each case was chosen to be a 90×90 structured, uniform grids. The estimator discretization was significantly coarser at just 30×30 computational points. These discretizations ensured high fidelity data was available from the forward problem, while still allowing the estimator to be calculated in real time. A computational time step of 0.1s was chosen for all simulations, which was significantly below the value dictated by stability requirements.

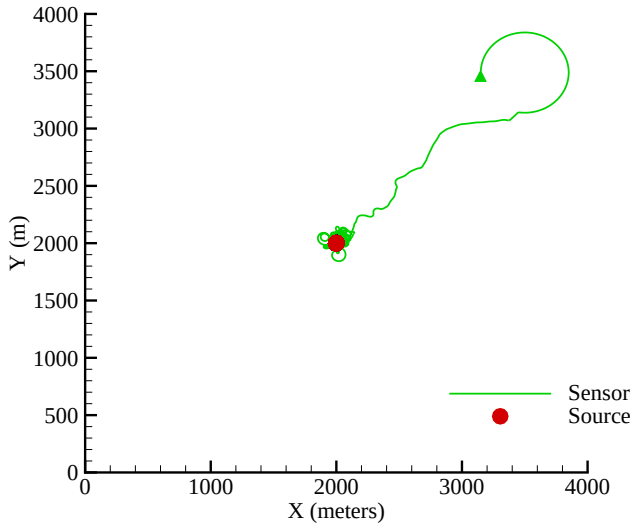

Figure 7: Trajectory of the sensor (green) and with a stationary source (red).

7.1 Stationary Source

A stationary source was simulated with a constant release rate in the center of the domain. Such a stationary source would be expected for a crash or leak situation. The entire $500s$ simulation took $187s$ to calculate. Figure 7 shows the trajectory of the sensor as it travels towards the source. At approximately $110s$, the sensor detected a nonzero concentration and begun the estimation process. As shown in Figure 8, the sensor got very close to the source in approximately $180s$. From the plot of the norm of the concentration error given in Figure 9, it can be seen that the norm is increasing until the sensor starts heading towards the source. The error norm then quickly falls. The error then fluctuates around a non-zero value, as is expected since the source is stationary and the sensor can not stop moving. As the SAV flies past the source, the state error at the location of the source increases until the sensor is driven back to the source location.

7.2 Crossing Source Trajectory

A crossing source trajectory was also considered. The source traveled directly across the diagonal of the domain, then traveled directly across the other diagonal. The source in this case had a maximum velocity of $15m/s$. The crossing source trajectory simulated $1450s$ and took $892s$ to compute. The trajectory of the source and sensor is shown in Figure 10. At approximately $200s$, the sensor detected the source and

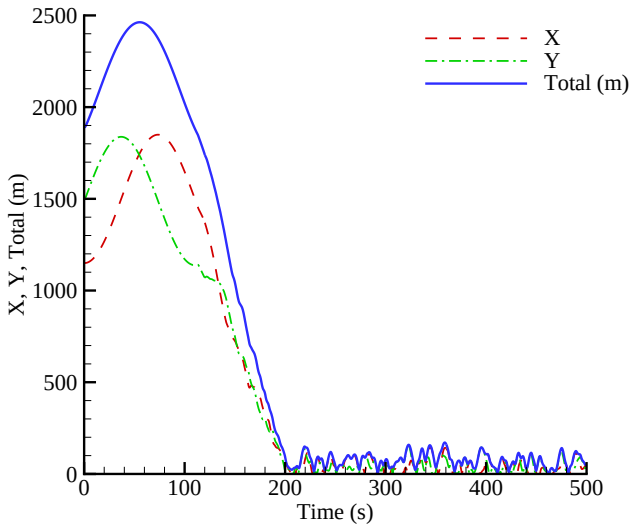

Figure 8: Distance between the source and sensor for a stationary source.

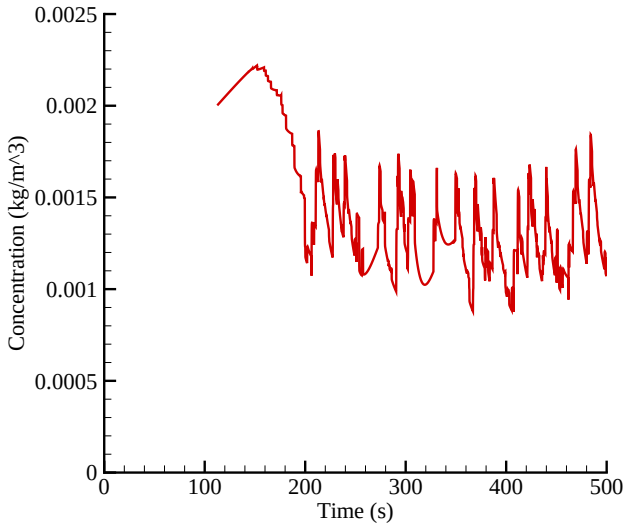

Figure 9: State error norm for a stationary source.

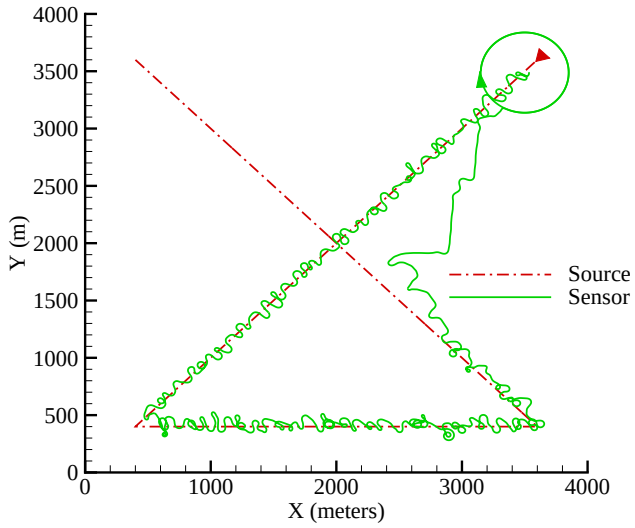

Figure 10: Trajectory of the sensor (green) and a crossing source trajectory (red).

begun the estimation process. Figure 11 shows that the sensor and source got very close in around $400s$. From the plot of the state error norm in Figure 12, the guidance scheme drives the state error towards zero. Fluctuations in the value were due to the fact that the sensor was constantly moving.

7.3 Circular Source Trajectory

A circular source trajectory was examined in the third simulation. Such a situation models a source releasing material over a designated area in order to cause damage to that area. The circular source trajectory simulated $500s$ and took $437s$ to compute. The source had a maximum velocity of $15m/s$. The trajectory of the source and sensor is shown in Figure 13.

Figure 14 shows the distance between the source and sensor as a function of time. The sensor remained close to the source for most of the trajectory, but wandered away at two points. The first was around $400s$. At this point, the sensor went too far towards the X-axis and initiated a spiral outward search to again find the plume. When it found the plume, it traveled downwind where there was a high state estimation error before heading towards the plume upwind. The second loss occurred around $550s$. Here, the sensor traveled too far towards the Y axis and lost the plume, but quickly returned toward the source. The state error norm plot is given in Figure 15. In both cases where the sensor lost the plume, the norm can be seen to increase a bit. However, the overall trend of the norm is driven towards zero, as desired.

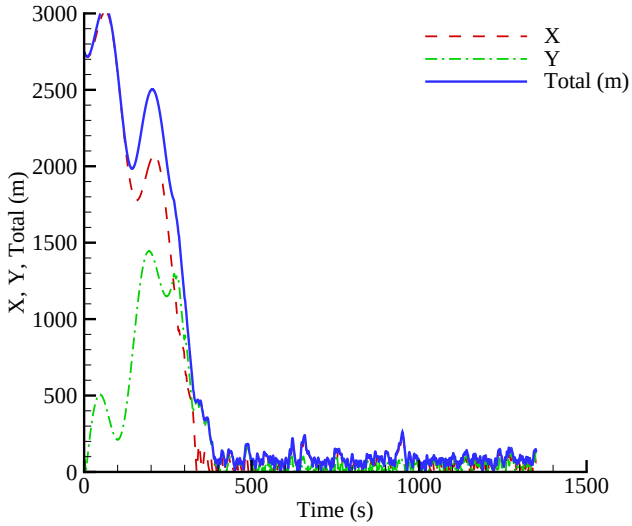

Figure 11: Distance between the sensor and a crossing source trajectory.

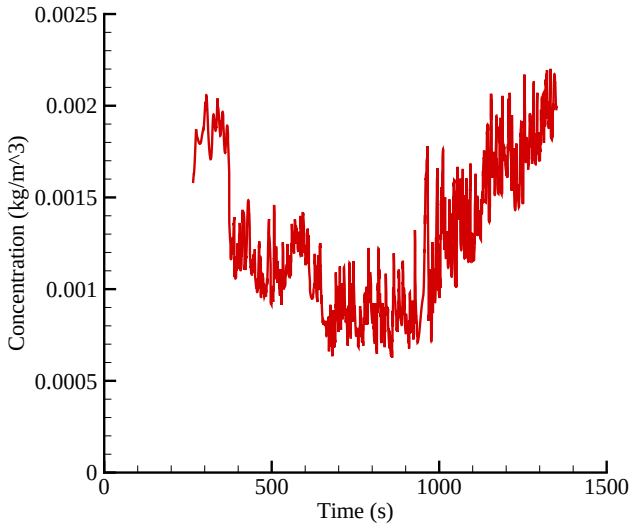

Figure 12: State error norm for a crossing source trajectory.

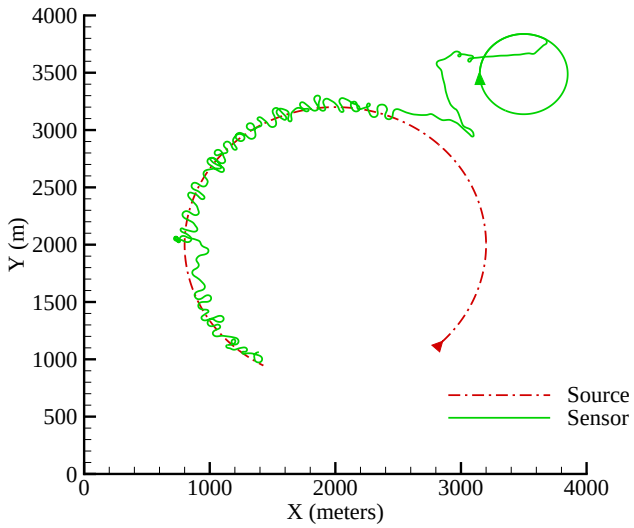

Figure 13: Trajectory of the sensor (green) and a circular source trajectory (red).

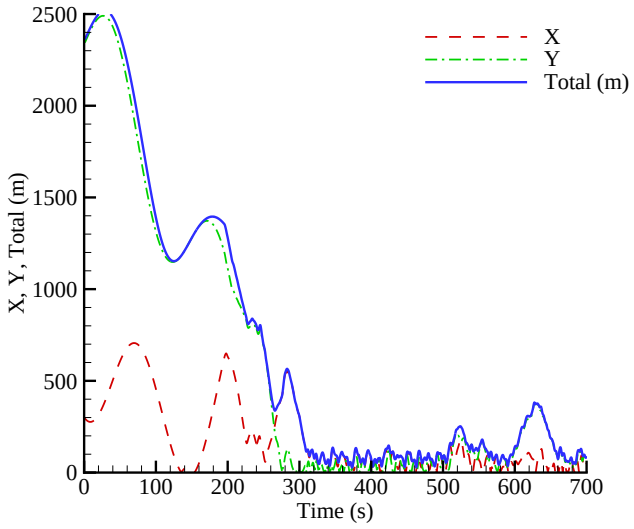

Figure 14: Distance between the sensor and a circular source trajectory.

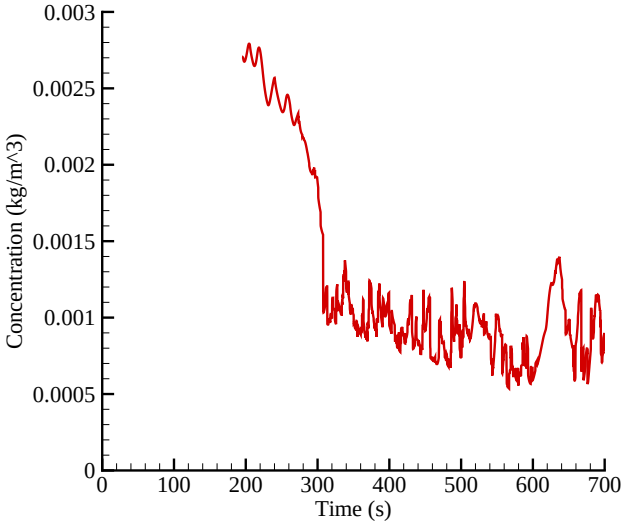

Figure 15: State error norm for a circular source trajectory.

7.4 Overlapping Source Trajectory

An overlapping source trajectory was simulated. This type of source would be applicable to an intruder doing surveillance over an area, or quickly entering an area to deposit material and quickly leave. The overlapping source trajectory simulated $700s$ and took $226s$ to compute. The maximum source velocity in this case was $18m/s$. The trajectory is shown in Figure 16. For this trajectory, the source followed the sensor very closely for the entire simulation. The sensor detected a nonzero concentration after $120s$ and quickly started following the source. The norm of the state error for this trajectory provided some interesting results. The norm was reduced as the source traveled through the first half of the trajectory. However, as the source traveled along the second half, it was traveling downwind. With the sensor slightly behind the source and the material from the source advecting downwind, the state error norm was slowly increasing, until the source stopped heading directly downwind in approximately $650s$. The norm then again continued to decline.

8 Conclusions

A model-based estimation scheme of a mobile gaseous source has successfully been considered for a 2D spatial domain. Such a spatial domain was assumed to be parallel to earth's surface. Using a mobile sensor

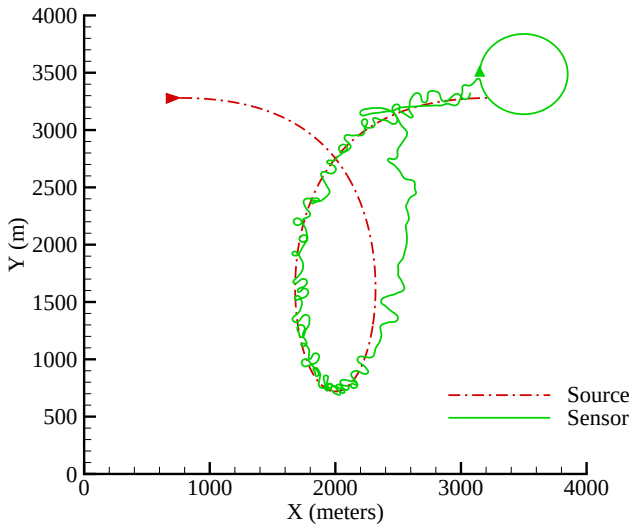

Figure 16: Trajectory of the sensor (green) and an overlapping source trajectory (red).

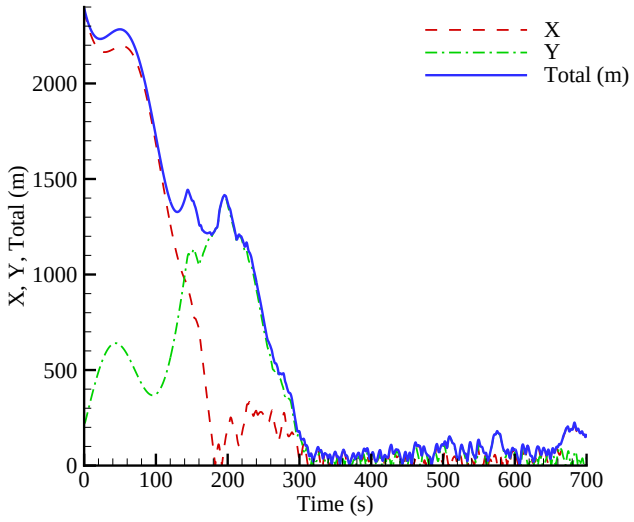

Figure 17: Distance between the sensor and an overlapping source trajectory.

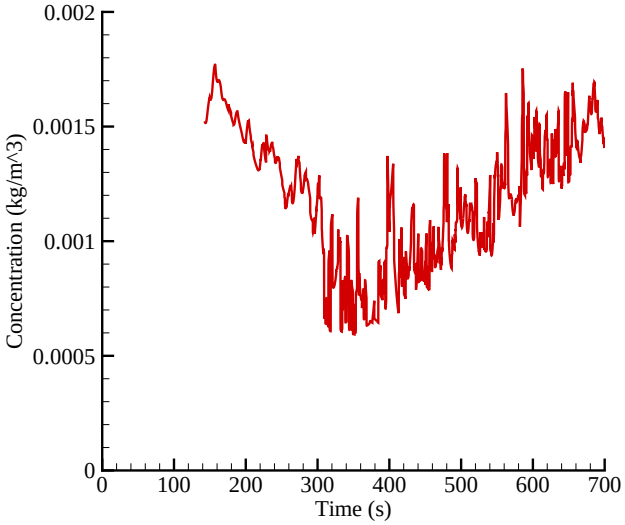

Figure 18: State error norm for an overlapping source.

on board an unmanned aerial vehicle (sensing aerial vehicle), the estimation scheme provided the spatial repositioning of the SAV in terms of control inputs (torques) to the SAV. Using Lyapunov methods, the model-based estimation scheme accounted for the dynamic motion of the SAV and provided its guidance in terms of the performance of the estimation scheme; thus the motion of the SAV *was solely dictated by the performance of the estimation scheme*. Such a scheme was essentially a (spatial) gradient scheme where the SAV was guided to the spatial regions of higher state estimation error or higher gradients of the estimation error.

While the infinite dimensional model of the physical process associated with the gaseous source had a fixed state operator, the state estimator, through its finite dimensional implementation, lend itself in state-dependent switching. This was made possible through different evaluations of the advection-diffusion operator over different grids. Multiple grids representing different coarser/refined grids of the 2D spatial domain, representing different regions of interest within the 2D spatial domain were used to evaluate the advection-diffusion operator. The resulting switched system switched to a different state matrix depending on the current location of the sensor. Thus, a *performance based switching that bridged computational fluid dynamics and controls* was considered in this research effort.

9 Personnel Supported

The following personnel were partially supported during the period of performance of this grant. The educational status at the time of their support as well as their current position is also indicated.

1. Dr. M.A. Demetriou, PI, Professor of Mechanical Engineering
2. Dr. N.A. Gatsonis, co-PI, Professor of Mechanical Engineering
3. Jeffrey Court, Ph.D. Candidate, Graduate Research Assistant (supported 06/09 - 11/11)
4. Raffaele Potami Post Doctoral Associate (partially supported, 6/09-11/09)
5. Jun Yang Ph.D. Candidate, Graduate Research Assistant (partially supported 6/09-8/09).

10 Publications

The following publications acknowledge support by this grant.

10.1 Journal and Conference Proceedings

1. J. Court, M.A. Demetriou and N.A. Gatsonis, Spatial gradient measurement through length scale estimation for the tracking of a gaseous source, accepted to the 2012 American Control Conference, Fairmont Queen Elizabeth, Montreal, Canada, June 27 - 29, 2012.
2. M.A. Demetriou, “Guidance of a moving sensor for the control of diffusion PDEs based on on-line approximations of feedback kernels”, accepted to the 2012 American Control Conference, Fairmont Queen Elizabeth, Montreal, Canada, June 27 - 29, 2012.
3. S.S. Nestinger and M.A. Demetriou,“Adaptive collaborative estimation of multi-agent mobile robotic systems”, accepted to the 2012 IEEE International Conference on Robotics and Automation, River Centre, Saint Paul, Minnesota, USA, May 14-18, 2012.
4. M.A. Demetriou, N.A. Gatsonis and J. Court, Lyapunov based guidance of a mobile sensing agent for state estimation of a gaseous source in a 3D spatial domain, Proceedings of the 50th IEEE Conference on Decision and Control and European Control Conference, Orlando, Fla, December 12-15, 2011.

5. M.A. Demetriou, “Adaptive consensus filters for collocated infinite dimensional systems”, Proceedings of the 50th IEEE Conference on Decision and Control and European Control Conference, Orlando, Fla, December 12-15, 2011.

6. M. A. Demetriou and S.S. Nestinger, “Adaptive consensus estimation of multi-agent systems, Proc. of the 50th IEEE Conference on Decision and Control and European Control Conference, Orlando, December 12-15, 2011.

7. M.A. Demetriou, N.A. Gatsonis and J. Court, “Model-based detection of a moving gaseous source in a 2D spatial domain using a sensor-based grid adaptation approach”, Proceedings of the 2011 American Control Conference, San Francisco, CA, June 29-July 1, 2011.

8. M.A. Demetriou, Simplified controller design for distributed parameter systems using mobile actuator with augmented vehicle dynamics, Proceedings of the 2011 American Control Conference, San Francisco, CA, June 29-July 1, 2011.

9. M.A. Demetriou and D. Ucinski, State estimation of spatially distributed processes using mobile sensing agents, Proceedings of the 2011 American Control Conference, San Francisco, CA, June 29-July 1, 2011.

10. M.A. Demetriou, N.A. Gatsonis and J. Court, Numerical investigation of the spatial estimation error in sensor guidance used for the localization of a gaseous source in a 2D domain, Proceedings of the 19th Mediterranean Conference on Control and Automation, Corfu, Greece, June 20-23, 2011.

11. M.A. Demetriou, Enforcing and enhancing consensus of spatially distributed filters utilizing mobile sensor networks, Proceedings of the 49th IEEE Conference on Decision and Control, Atlanta, GA, December 15-17, 2010.

12. M.A. Demetriou, Overview of consensus filters for distributed parameter systems utilizing sensor networks, Proc. of the Nineteenth International symposium on Mathematical Theory of Networks and Systems (MTNS2010), Budapest, Hungary, July 5-9, 2010.

13. M.A. Demetriou, “Measure of disagreement of spatially distributed filters for distributed parameter systems”, Proc. of the 2010 American Control Conference, Baltimore, Maryland, USA June 30 - July 2, 2010.

14. M.A. Demetriou, “Design of spatially distributed filters for distributed parameter systems using mobile sensor networks”, Proc. of the 2010 American Control Conference, Baltimore, Maryland, USA June 30 - July 2, 2010.

15. M.A. Demetriou, “Controlling distributed parameter systems using mobile actuator-plus-sensor networks”, Proc. of the 48th IEEE Conference on Decision and Control, Shanghai, P.R. China, December 16-18, 2009.

16. M.A. Demetriou, Enforcing consensus on adaptive parameter estimation of structurally perturbed infinite dimensional systems, under review, IEEE Transactions on Automatic Control, Feb. 2011.

17. M.A. Demetriou, N.A. Gatsonis and J. Court, Detection of moving gaseous source in 2D domains using a mobile sensor and a grid-based hybrid estimator dynamics, submitted to IEEE Transactions on Control Systems Technology.

18. M.A. Demetriou, N.A. Gatsonis and J. Court, Guidance of a sensing aerial vehicle in 3D domain used for the estimation of a moving gaseous source, under preparation, to be submitted to AIAA J. Guidance, Control and Dynamics, spring 2012.

10.2 Dissertations

1. J. Court, “Detection of a moving gaseous source via a model-based estimation scheme with a sensing aerial vehicle”, Ph.D. Dissertation, expected May, 2012.

References

[1] J. H. Seinfeld and S. N. Pandis, *Atmospheric Chemistry and Physics: From Air Pollution to Climate Change*. New York: Wiley-Interscience, 2006.

[2] S. P. Arya, *Air Pollution Meteorology and Dispersion*. New York: Oxford University Press, 1999.

[3] R. A. Dobbins, *Atmospheric Motion and Air Pollution*. New York: Wiley, 1979.

[4] K. Brzozowski and W. Kotlarz, “Modelling of air pollution on a military airfield,” *Atmospheric Environment*, vol. 39(33), pp. 6130–6139, 2005.

[5] N. Koutsourakis, J. Bartzis, A. Venetsanos, and S. Farailidis, "Computation of pollutant dispersion during an airplane take-off," *Environmental Modelling & Software*, vol. 21(4), pp. 486 – 493, 2006.

[6] C. Hirsch, *Numerical Computation of Internal & External Flows*. Oxford, GB: Butterworth-Heinemann, 2007.

[7] N. A. Gatsonis, M. Demagistris, and R. Erlandson, "Three-dimensional magnetohydrodynamic modeling of plasma jets in north star space experiment," *Journal of Spacecraft and Rockets*, vol. 41, no. 4, pp. 509–520, July Aug 2004.

[8] D. R. Lynch, *Numerical Partial Differential Equations for Environmental Scientists and Engineers*. New York: Springer, 2005.

[9] M. Ram and V. Bhethanabotla, *Sensors for Chemical and Biological Applications*. New York: CRC Press, 2010.

[10] E. Cespedes and C. Kolb, "Spectroscopic environmental trace species sensors," *Optics & Photonics ews*, vol. 9(8), pp. 38–43, August 1998.

[11] M. Ghanem, Y. Guo, J. Hassard, M. Osmond, and M. Richards, "Sensor grids for air pollution monitoring," in *In Proc. 3rd UK e-Science All Hands Meeting*, 2004.

[12] U. Schumann, H. Schlager, F. Arnold, R. Baumann, P. Haschberger, and O. Klemm, "Dilution of aircraft exhaust plumes at cruise altitudes," *Atmospheric Environment*, vol. 32, no. 18, pp. 3097 – 3103, 1998.

[13] R. A. Adams, *Sobolev Spaces*. NY: Academic Press, 1975.

[14] R. F. Curtain and H. J. Zwart, *An Introduction to Infinite Dimensional Linear Systems Theory*, ser. Texts in Applied Mathematics, Vol. 21. Berlin: Springer-Verlag, 1995.

[15] R. Temam, *Infinite Dimensonal Dynamical Systems in Mechanics and Physics*, 2nd ed. New York: Springer-Verlag, 1997.

[16] G. Duvaud and J. Lions, *Inequalities in Mechanics & Physics*. New York: Springer-Verlag, 1976.

[17] J. L. Lions and E. Magenes, *Non-Homogeneous Boundary Value Problems, I*. New York: Springer-Verlag, 1972.

[18] M. A. Demetriou, "Guidance of mobile actuator-plus-sensor networks for improved control and estimation of distributed parameter systems," *IEEE Tr. on Automatic Control*, vol. 55(7), pp. 1570–1584, 2010.

[19] U. Schumann, H. Schlager, F. Arnold, J. Ovarlez, H. Kelder, O. Hov, G. Hayman, I.S.A.Isaksen, J. Staehelin, and P. Whitefield, "Pollution from aircraft emissions in the north atlantic flight corridor: Overview on the polinat projects," *Journal of Geophysical Research*, vol. 105(D3), pp. 3605–3631, February 2000.

[20] U. Schumann, P. Konopka, R. Baumann, R. Busen, T. Gerz, H. Schlager, P.Schulte, and H. Volkert, "Estimate of diffusion parameters of aircraft exhaust plumes near the tropopause from nitric oxide and turbulence measurements," *Journal of Geophysical Research*, vol. 100(D7), pp. 14,147–14,162, July 1995.

[21] R. B. Bird, W. E. Stewart, and E. N. Lightfoot, *Transport Phenomena*. New York: John Wiley & Son, 2007.

[22] Z. Ya, P. Bhattacharya, H. Mohamadian, H. Majlesein, and Y. Ye, "Equational dynamic modeling and adaptive control of uav," in *Proc. of the 2006 IEEE/SMC International Conf. on System of Systems Engineering*, Los Angels, CA, April 2006.

[23] R. Fierro and F. Lewis, "Control of a nonholonomic mobile robot: Backstepping kinematics into dynamics," *Journal of Robotic Systems*, vol. 14(3), pp. 149–164, 1997.

[24] A. M. loch, M. Reyhanoglu, and N. H. McClamroch, "Control and stabilization of nonholonomic dynamic systems," *IEEE Trans. Autom. Control*, vol. 37(11), pp. 1746–1757, 1992.

[25] A. Gholipour and M. Yazdanpanah, "Dynamic tracking control of nonholonomic mobile robot with model reference adaptation for uncertain parameters," in *Proc. of the 2003 European Control Conference*, Cambridge, UK, September 2003.

[26] I. Kolmanovsky and N. H. McClamroch, "Developments in nonholonomic control problems," *IEEE Contr. Syst. Technol. Mag.*, vol. 15, pp. 20–36, December 1995.

[27] W. Ren and R. W. Beard, "Clf-based tracking control for uav kinematic models with saturation constraints," in *Proc. of the 42nd IEEE Conference on Decision and Control*, Maui, HI, December 2003.

[28] G. P. Roussos, D. V. Dimarogonas, and K. J. Kyriakopoulos, "3d navigation and collision avoidance for a non-holonomic vehicle," in *Proc. of the 2008 American Control Conf.*, Seattle, WA, June 2008.

[29] W. Ren and R. W. Beard, "Trajectory tracking for unmanned air vehicles with velocity and heading rate constraints," *IEEE Tr. on Contr. Sys. Tech.*, vol. 12(5), pp. 706–716, Sept. 2004.

[30] B. Etkin, *Dynamics of Flight*. New York: Wiley, 1996.

[31] B. Stevens and F. Lewis, *Aircraft Control and Simulation*. London: J. Wiley, 2003.

[32] M. A. Demetriou, N. A. Gatsonis, and J. R. Court, "Model-based detection of a moving gaseous source in a 2d spatial domain using a sensor-based grid adaptation approach," in *Proc. of the 2011 American Control Conf.*, San Francisco, CA, June 29- July 1 2011, pp. 2374–2380.

[33] ——, "Numerical investigation of the spatial estimation error in sensor guidance used for the localization of a gaseous source in a 2d domain," in *Proc. of the 19th Mediterranean Conference on Control and Automation*, Corfu, Greece, June 20-23 2011.

[34] J. Kaipio and E. Somersalo, *Statistical and Computational Inverse Problems*. New York: Springer, 2005.

[35] W. Briggs, *A Multigrid Tutorial*. Philadelphia: Society for Industrial and Applied Mathematics, 2000.

[36] G. Carey and A. Pardhanani, "Multigrid solution and grid redistribution for convection-diffusion," *International Journal for Numerical Methods in Engineering*, vol. 27, pp. 655–664, September 1989.

[37] D. Liberzon, *Switching in Systems and Control*. Boston: Birkhäuser, 2003.